A COMPREHENSIVE EVALUATION OF RESERVOIR INFLOW AND WELLBORE BEHAVIOR IN INTELLIGENT WELLS

A Thesis

by

MARWAN ANNAS H ZAREA

Submitted to the Office of Graduate Studies of
Texas A&M University
in partial fulfillment of the requirements for the degree of

MASTER OF SCIENCE

August 2010

Major Subject: Petroleum Engineering

A Comprehensive Evaluation of Reservoir Inflow and

Wellbore Behavior in Intelligent Wells

Copyright 2010 Marwan Annas H Zarea

A COMPREHENSIVE EVALUATION OF RESERVOIR INFLOW AND WELLBORE BEHAVIOR IN INTELLIGENT WELLS

A Thesis

by

MARWAN ANNAS H ZAREA

Submitted to the Office of Graduate Studies of
Texas A&M University
in partial fulfillment of the requirements for the degree of

MASTER OF SCIENCE

Approved by:

Co-Chairs of Committee,	Ding Zhu
	Walter B. Ayers
Committee Member,	Francis J. Narcowich
Head of Department,	Stephen A. Holditch

August 2010

Major Subject: Petroleum Engineering

ABSTRACT

A Comprehensive Evaluation of Reservoir Inflow and Wellbore Behavior in Intelligent Wells. (August 2010)

Marwan Annas H Zarea, B.S., Montana Tech of the University of Montana

Co-Chairs of Advisory Committee: Dr. Ding Zhu
Dr. Walter B. Ayers

Intelligent well technology is a relatively new technology that has been adopted by many operators in recent years to improve oil and gas recovery. Because of its complexity, accurate modeling of the reservoir and wellbore performance in the multilateral well application is critical to optimize well production. Little work has been performed on understanding the flow behavior through the main component of the intelligent well, the inflow control valve. This study presents a comprehensive model to quantify the reservoir and well performance in the horizontal laterals of the intelligent multilateral well. Moreover, it combines this model with equations to evaluate the flow rate and pressure profile through the inflow control valves. As a result of this study, the well performance of intelligent wells can be predicted and optimized.

DEDICATION

To my great parents, lovely wife, and best brothers and sister for their continuous love and support

ACKNOWLEDGEMENTS

Praise and gratitude to Allah, the Almighty, for the abundant mercies and blessings, and to his Prophet Mohammed, peace be upon him.

I would like to express my gratitude to the management of Saudi Aramco for their great support in providing me with a scholarship to pursue my graduate studies in Texas A&M University.

I would like to thank my committee co-chairs, Dr. Ding Zhu and Dr. Walter B. Ayers, for their continuous encouragement and academic guidance throughout the course of this research.

I would also like to thank my committee member, Francis J. Narcowich, for the valuable comments and suggestions that have shaped the work in this thesis.

Thanks also go to my friends and colleagues in the research group for the constructive discussions, and to the department faculty and staff for making my time at Texas A&M University a great experience.

Finally, thanks to my mother and father for their encouragement and to my wife for her patience and love.

TABLE OF CONTENTS

Page

LIST OF FIGURES

LIST OF TABLES

1. INTRODUCTION

1.1 Background

The trend of increasing hydrocarbon demand is faced with a decrease in new discoveries; hence, the need to enhance productivity from existing fields and improve their ultimate recovery is an imposing challenge for producers. Horizontal drilling and well completion technologies have seen rapid developments in the last decade to address this issue.

The concept of Maximum Reservoir Contact (MRC) wells was introduced in 2002 in the Middle East and has been applied mainly in reservoirs with tight rock and relatively thin oil columns. An MRC well is defined as a well with an aggregate reservoir contact in excess of 5 kilometers, through a single or multi-lateral well configuration (Salamy et al. 2008). MRC wells provide improved well performance and enhanced oil recovery. In addition, they are a more cost-effective alternative to conventional wells in terms of a reduced unit cost of drilling ($/ft) and production ($/bbl). With the use of MRC wells, the total number of wells and their associated surface facilities can be significantly reduced in a field's development (Dossary and Mahgoub 2003).

Intelligent completion is a technology that was developed primarily to provide means to improve recovery from existing fields. It consists of downhole valves referred to as inflow control valves (ICV), also known as interval control valves, to selectively

---

This thesis follows the style of *SPE Journal.*

control the flow of different segments in a single lateral horizontal well or commingled production from different laterals in a multilateral well. An intelligent completion can be equipped with permanent downhole measurement equipment which transmits real-time pressure and temperature data to the engineer's desktop. The genesis of the intelligent well era was marked by the first successful installation of intelligent completions in 1997 in the Norwegian part of the North Sea (Konopczynski and Ajayi 2008). Due to its proven capabilities, many companies have heavily implemented this technology during the last decade. In 2004, Saudi Aramco coupled intelligent completions with its multilateral MRC wells to manage and optimize production from different laterals. Field results have shown direct advantage of using ICVs over conventional wells in terms of improving overall productivity and sweep, managing water production and minimizing production interruptions (Mubarak et al. 2009).

1.2 Literature Review

Many models have been published to evaluate the well performance in horizontal wells. These models are classified based on the flow condition as either steady-state or pseudo-steady-state. Joshi (1988) presented a model for steady-state flow condition assuming an elliptical drainage area. He handled the three-dimensional flow problem by separating the horizontal flow into x-y plane and y-z plane and treating them separately. Butler (1994) and Furui (2003) presented steady-state models for box-shaped reservoirs. Their models yield very similar results, although they are derived by different approaches. Butler's model was based on the image well superposition technique,

whereas Furui's model was based on the finite element model. On the other hand, Babu and Odeh (1989) presented a pseudo-steady-state model that is widely used for horizontal well productivity. The model assumes a box-shaped reservoir and a well parallel to the x-direction. All the above models are for incompressible or slightly compressible single-phase liquid; however, they can be extended to other fluid types.

Little work has been presented on modeling the flow across the inflow control valves. In general, ICVs can be treated as surface chokes with minor modifications to account for downhole conditions. Various studies describing two-phase flow through chokes have been published. Sachdeva et al. (1986) and Perkins (1993) models are representative of most of these works. They both describe the flow conditions under critical and subcritical flow and are based on the equations for conservation of mass, momentum and energy.

1.3 Objectives of Research

The objectives of this study are to predict and optimize the well performance of unconventional wells such as the multilateral MRC wells that are equipped with intelligent completions. This study will result in models and procedures to evaluate horizontal well performance and pressure drop across ICVs for both single-phase and two-phase flow.

1.4 Methodology

Modeling intelligent wells requires accounting for reservoir, wellbore and completion performance effects. To meet this objective, existing models to predict the reservoir and wellbore behavior along with equations that can predict the flow performance through restrictions such as the ICV are integrated. The integrated model estimates the reservoir inflow and flowing wellbore pressure at each lateral of the intelligent well, then predicts the anticipated pressure drop across each ICV for any given flow rate, therefore, enabling the selection of the proper ICV position for each lateral or segment to optimize the well production.

2. MODELING OF HORIZONTAL LATERALS

2.1 Reservoir Inflow Model

The performance of a horizontal well can be predicted by first determining the reservoir inflow behavior in the lateral. To achieve this objective, either the analytical or reservoir simulation modeling technique can be used. Both techniques predict the flow rate in the lateral as a function of pressure drawdown. Although the reservoir simulation models are considered more accurate in predicting the well performance, analytical models are an attractive alternative in the field because they require less input, effort and time, especially when working on designing and optimizing the performance of a single well. In this study, only the analytical modeling approach will be discussed.

The analytical models for horizontal wells are referred to as the inflow performance relationship (IPR) equations. In horizontal wells, IPR equations are categorized based on the boundary conditions into steady-state flow condition where the pressure at the boundary is constant and pseudo-steady-state flow condition where there is no flow at the boundary (Kamkom and Zhu 2006).

2.1.1 Single-Phase Oil Wells

The flow rate for a single-phase slightly-compressible fluid, such as oil, can be described based on the boundary conditions by either steady-state or pseudo-steady-state conditions. Babu and Odeh (1989) presented a pseudo-steady-state IPR model for a horizontal well where the reservoir is bounded by no flow boundaries and the pressure

declines at a constant rate. The model was derived by rotating a vertical well to represent a horizontal well and adding a geometry factor to account for the change in drainage area. Babu and Odeh's model assumes a box shaped drainage area with a reservoir length in the x-direction and width in the horizontal y-direction perpendicular to the wellbore (**Figure 2.1**).

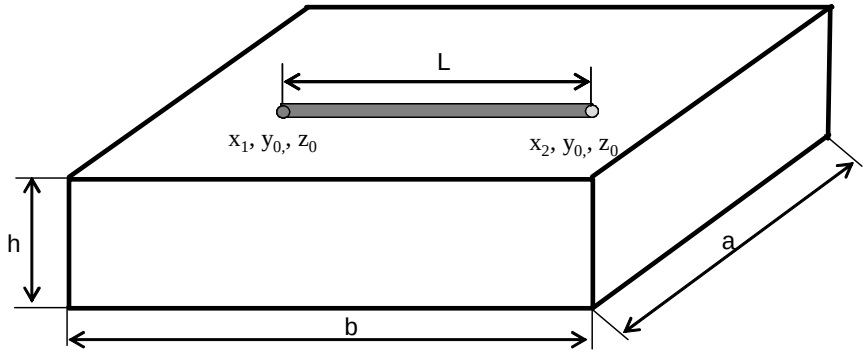

Figure 2.1: Schematic of Babu and Odeh's model (Hill et al. 2008).

The horizontal wellbore extends parallel to the x-direction and can be at any arbitrary location in the reservoir. However, the model imposes some constraints for the wellbore not to be too close to any of the reservoir boundaries. This is governed by some conditional equations in the model as will be presented. The model uses a partial penetration skin factor to account for the inflow from the reservoir beyond the ends of the wellbore in the x-direction (Hill et al. 2008). The inflow equation presented in this model follow the most familiar form for that of a vertical well. Thus, the Babu and Odeh inflow equation for a horizontal well is represented by

$$q = \frac{\sqrt{k_y k_z}\, b\left(\bar{p} - p_{wf}\right)}{141.2 B_o \mu \left[\ln\left(\frac{A^{0.5}}{r_w}\right) + \ln C_H - 0.75 + s_R + s\right]} \tag{2.1}$$

where in **Eq. 2.1**, C_H is the shape factor and s_R is the partial penetration skin factor. The skin factor, s, represents any other skins, such as formation or completion skin effects.

Babu and Odeh derived simplified equations to calculate the shape factor, C_H, and the partial penetration skin, s_R, which are needed in the solution of the horizontal well inflow equation.

$$\ln C_H = 6.28 \frac{a}{h} \sqrt{\frac{k_z}{k_y}} \left[\frac{1}{3} - \frac{y_0}{a} + \left(\frac{y_0}{a}\right)^2\right] - \ln\left(\sin\frac{\pi z_0}{h}\right) - 0.5 \ln\left[\left(\frac{a}{h}\right)\sqrt{\frac{k_z}{k_y}}\right] - 1.088 \tag{2.2}$$

Eq. 2.2 can be written in terms of the anisotropy ratio, I_{ani}, which is defined as

$$I_{ani} = \sqrt{\frac{k_H}{k_V}}$$

Thus, **Eq. 2.2** becomes

$$\ln C_H = 6.28 \frac{a}{I_{ani} h} \left[\frac{1}{3} - \frac{y_0}{a} + \left(\frac{y_0}{a}\right)^2\right] - \ln\left(\sin\frac{\pi z_0}{h}\right) - 0.5 \ln\left[\left(\frac{a}{I_{ani} h}\right)\right] - 1.088 \tag{2.3}$$

As mentioned, the partial penetration skin factor accounts for any inflow beyond the ends of the wellbore. Therefore, s_R is equal to zero if the horizontal well is fully penetrating the reservoir, i.e., when the wellbore length, L, equals the reservoir drainage length, b. On the other hand, when the wellbore is partially penetrated, i.e., the wellbore length is shorter than the drainage length, s_R is calculated for two different cases

depending on the drainage geometry and permeability anisotropy. The first case is for a relatively wide reservoir, where if the following criteria are met

$$\frac{a}{\sqrt{k_x}} \geq 0.75\frac{b}{\sqrt{k_y}} > 0.75\frac{h}{\sqrt{k_z}},$$

we have

$$s_R = P_{xyz} + P'_{xy} \tag{2.4}$$

where

$$P_{xyz} = \left(\frac{b}{L} - 1\right)\left[\ln\frac{h}{r_w} + 0.25\ln\frac{k_y}{k_z} - \ln\left(\sin\frac{\pi z}{h}\right) - 1.84\right] \tag{2.4a}$$

$$P'_{xy} = \frac{2b^2}{Lh}\sqrt{\frac{k_z}{k_x}}\left\{F\left(\frac{L}{2b}\right) + 0.5\left[F\left(\frac{4x_{mid} + L}{2b}\right) - F\left(\frac{4x_{mid} - L}{2b}\right)\right]\right\} \tag{2.4b}$$

The second case is for a relatively long reservoir, where if the following criteria are met

$$\frac{b}{\sqrt{k_y}} \geq 1.33\frac{a}{\sqrt{k_x}} > \frac{h}{\sqrt{k_z}},$$

we have

$$s_R = P_{xyz} + P_y + P_{xy} \tag{2.5}$$

where

$$P_y = \frac{6.28b^2}{ah}\frac{\sqrt{k_y k_z}}{k_x}\left[\left(\frac{1}{3} - \frac{x_{mid}}{b} + \frac{x_{mid}^2}{b^2}\right) + \frac{L}{24b}\left(\frac{L}{b} - 3\right)\right] \tag{2.5a}$$

$$P_{xy} = \left(\frac{b}{L} - 1\right)\left(\frac{6.28a}{h}\sqrt{\frac{k_z}{k_y}}\right)\left(\frac{1}{3} - \frac{y_0}{a} + \frac{y_0^2}{a^2}\right) \tag{2.5b}$$

The functions in **Eq. 2.4b** are defined as

$$F(x)=\begin{cases} -(x)\left[0.145+\ln(x)-0.137(x)^2\right] \text{ for } x=\dfrac{L}{2b},\ x=\dfrac{4x_{mid}\pm L}{2b}\le 1 \\ (2-x)\left[0.145+\ln(2-x)-0.137(2-x)^2\right] \text{ for } x=\dfrac{4x_{mid}\pm L}{2b}>1 \end{cases}$$

The term x_{mid} represents the midpoint of the well on the x-coordinate and can be evaluated by

$$x_{mid}=\frac{x_1+x_2}{2}$$

If none of the criteria in the first and second cases are met, then the Babu and Odeh's model is not applicable to handle the given reservoir conditions.

2.1.2 Two-Phase Wells

Analytical inflow relationships that predict the performance of two-phase flow were first developed for vertical wells. Correlations were used to overcome the complexities encountered with two-phase flow due to relative permeability. Vogel (1968) presented an empirical equation for use in two-phase IPR calculations in vertical wells. The equation is

$$\frac{q_o}{q_{o,\max}}=1-0.2\left(\frac{p_{wf}}{\overline{p}}\right)-0.8\left(\frac{p_{wf}}{\overline{p}}\right)^2 \tag{2.6}$$

where p_{wf} and $\overline{p}$ are flowing bottomhole pressure and average reservoir pressure, respectively. $q_{o,max}$ is the production rate for single-phase oil flow at the maximum drawdown, i.e., when $p_{wf} = 0$.

Predicting the inflow performance for two-phase in horizontal wells is different than in vertical wells. The most important differences between the two are; first, in horizontal wells, the streamline consists of both radial and linear flow, whereas only radial flow presents in vertical wells; and second, the inflow performance in horizontal wells depends on both vertical and horizontal permeabilities, unlike vertical wells where only horizontal permeability presents. Therefore, the reservoir's anisotropy ratio is important when modeling the inflow performance of a horizontal well. These factors along with the relative permeability in two-phase reservoirs pose a challenge to obtain analytical models which can predict the performance of two-phase inflow in horizontal wells (Kamkom and Zhu 2005a).

Many researchers have developed correlations for two-phase inflow in horizontal wells by adopting the same methods presented in Vogel's two-phase inflow equation for vertical wells. Kabir (1992) presented a modified form of Vogel's correlation which estimates the absolute open flow potential for oil in a horizontal well, $q_{o,max}$, in terms of the productivity index, J. To derive his equation, Kabir differentiated Vogel's equation which results in

$$-\frac{dq_o}{dp_{wf}} = q_{o,\max}\left(0.2\frac{1}{\bar{p}} + 1.6\frac{p_{wf}}{(\bar{p})^2}\right) \tag{2.7a}$$

where the expression $\left(-dq_o/dp_{wf}\right)$ represents the productivity index. The maximum value the productivity index can have is when the values of p_{wf} and $\bar{p}$ are equal. Therefore, when ($p_{wf} = \bar{p}$), **Eq. 2.7a** can be written as

$$J = q_{o,\max}\left(1.8\frac{1}{p}\right) \tag{2.7b}$$

$q_{o,max}$ is solved in terms of the productivity index which is calculated by using any single-phase analytical model such as the Babu and Odeh model as shown in **Eq. 2.8**

$$J = \frac{q_o}{\overline{p} - p_{wf}} = \frac{b\sqrt{k_y k_z}}{141.2 B_o \mu\left[\ln\left(\frac{A^{0.5}}{r_w}\right) + \ln C_H - 0.75 + s_R + s\right]} \tag{2.8}$$

Finally, the gas flow rate can be calculated directly if the gas-oil ratio (GOR) is known

$$q_g = q_o(GOR) \tag{2.9}$$

2.2 Wellbore Flow Model

The pressure drop along the lateral can sometimes be significant in modeling the performance of a well. Several experimental and analytical studies have been performed to investigate the wellbore flow behavior for single-phase flow in horizontal wells. On the other hand, modeling the behavior of two-phase flow in horizontal wells by calculating the pressure drop and holdup is very challenging because it requires determining the different flow patterns or flow regimes associated with the gas-liquid flow along the wellbore (Ouyang et al. 1998).

Pressure drop calculation in producing laterals is different than that in standard pipes due to the presence of kinetic energy induced by inflow effects. In reservoirs with high productivity, high flow rates inside the laterals create considerable pressure drop especially when the reservoir drawdown is small. This becomes more significant in high-

permeability reservoirs with small diameter and long horizontal wellbores. Hence, the pressure drop effects must be accounted for when modeling wellbore flow. For a single-phase incompressible liquid, the pressure drop for a segment of length L_s that has an inclination of θ degrees from the horizontal axis is given by

$$\Delta p = p_1 - p_2 = \frac{g}{g_c}\rho L_s \sin\theta + \frac{2 f_f \rho u^2 L_s}{g_c d} \tag{2.10}$$

where the angle θ is positive for upwards flow, negative for downwards flow and zero for horizontal flow. **Eq. 2.10** represents the pressure drop for a standard pipe without any explicit term directly identifying the inflow effect on lateral pressure drop.

Many researchers have studied the pressure drop caused by radial inflow through perforations or slots in horizontal wellbores. Ouyang et al. (1998) presented a general single-phase wellbore flow model for pressure drop calculations accounting for frictional, accelerational and gravitational pressure drop effects which can be applied to horizontal, vertical and slanted wells. The model also accounts for pressure drop along the wellbore caused by inflow through perforations by including an empirical wall-friction-factor correlation in the frictional pressure drop term of the model. The inflow or mass transfer along the wellbore can be through perforations or pores in the wall as in openhole completions. The concept for both mass transfer media is identical since in the case of openhole completions, the wall is assumed to have infinite number of effective perforations or pores.

The pressure drop for a wellbore segment with a uniform inflow per unit length (**Figure 2.2**) is given by

$$\Delta p = p_1 - p_2 = \frac{g}{g_c}\rho L_s \sin\theta + \frac{2 f_f^* \rho u^2 L_s}{g_c d} + \frac{8\rho u q_I L_s}{\pi g_c d^2} \tag{2.11}$$

where f_f^* is the inflow wall friction factor and is defined for laminar flow as

$$f_f^* = \frac{16}{N_{\mathrm{Re}}}\left[1 + 0.04304 N_{\mathrm{Re},w}^{0.6142}\right] \tag{2.12}$$

and for turbulent flow as

$$f_f^* = f_f\left[1 - 0.0153\, N_{\mathrm{Re},w}^{0.3978}\right] \tag{2.13}$$

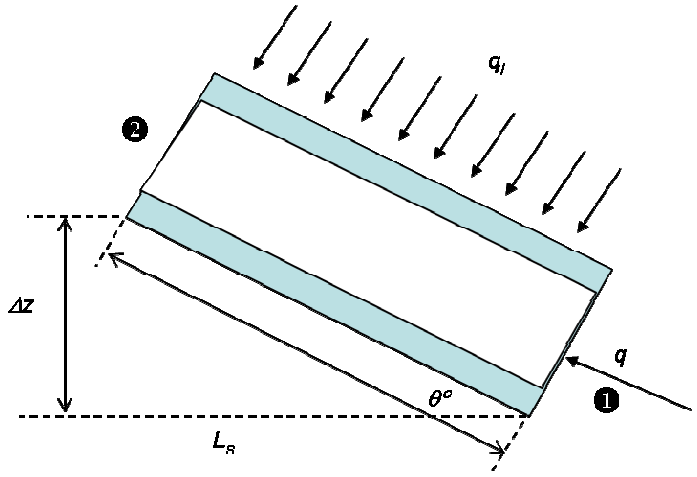

Figure 2.2: Wellbore flow geometry (Hill et al. 2008).

A common reference number to distinguish between laminar and turbulent flow is defined as the critical Reynolds number, $N_{Re,c}$ = 2100, where it represents the transition from laminar to turbulent flow in circular pipes. The value can vary slightly depending on the pipe roughness and other factors (Guo et al. 2007). In the case of

laminar flow, the inflow increases the wall friction factor, while for turbulent flow, the wall friction factor decreases by the inflow.

The term, $N_{Re,w}$, in **Eq. 2.12** and **2.13** is the injection wall or inflow Reynolds number, which is based on pipe inner diameter, and the inflow rate per unit wellbore length, q_I. $N_{Re,w}$ is defined by

$$N_{\mathrm{Re},w} = \frac{q_I \rho}{\pi \mu} \tag{2.14}$$

N_{Re} is the pipe flow Reynolds number and is given by

$$N_{\mathrm{Re}} = \frac{du\rho}{\mu} \tag{2.15}$$

The term, u, is the axial component of inflow velocity which is given by

$$u = \frac{4\bar{q}}{\pi d^2} \tag{2.16}$$

where $\bar{q}$ is the average flow rate in the wellbore segment and it is calculated by

$$\bar{q} = q + \frac{L_s}{2} q_I \tag{2.17}$$

(Hill et al. 2008).

The fanning friction factor or the no-wall-flow friction factor, f_f, can be obtained manually from charts such as the Moody friction factor diagram (**Figure 2.3**). This chart was generated from the implicit Colebrook-White equation which requires an iterative procedure to find a solution for the friction factor. However, there are a number of explicit approximation equations that take the form of the Colebrook-White equation and

produce similar accuracy for the friction factor. One of these equations is the Chen equation

$$\frac{1}{\sqrt{f_f}} = -4\log\left\{\frac{\varepsilon}{3.7065} - \frac{5.0452}{N_{\mathrm{Re}}}\log\left[\frac{\varepsilon^{1.1098}}{2.8257} + \left(\frac{7.149}{N_{\mathrm{Re}}}\right)^{0.8981}\right]\right\} \tag{2.18}$$

(Economides et al. 1993).

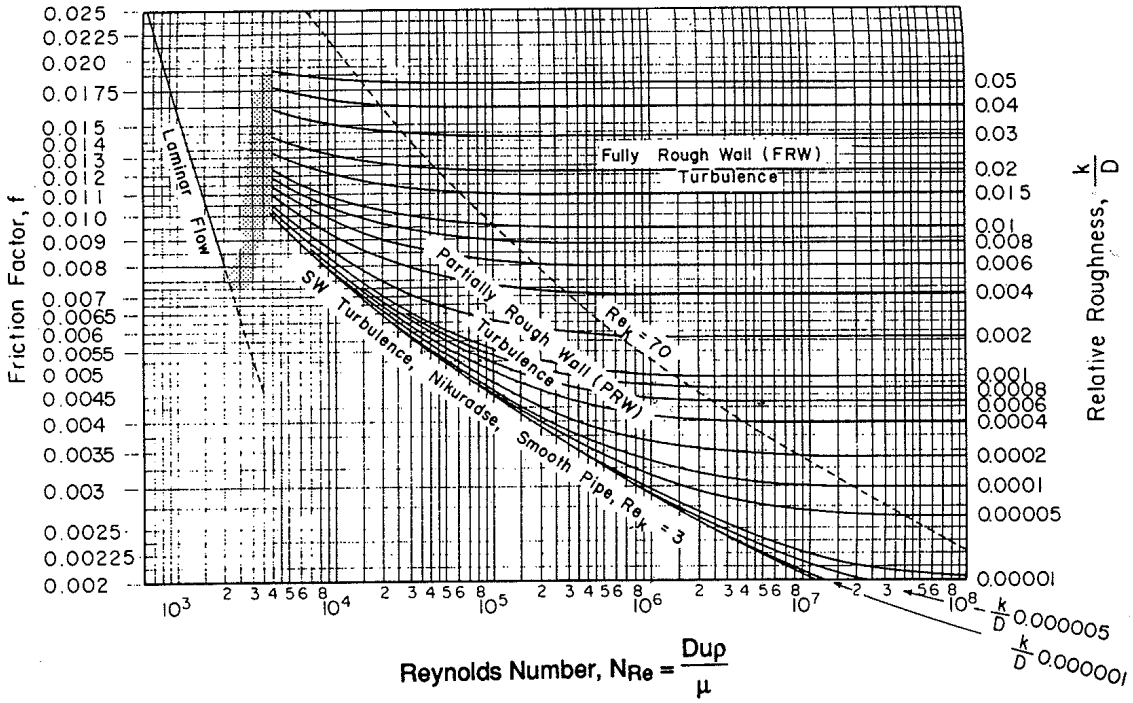

Figure 2.3: Moody diagram for friction factor (Economides et al. 1993).

Evaluation of pressure drop in build sections is essential when modeling wellbore flow. In some multilateral well configurations, build sections connect each lateral to the main wellbore where the flow from all laterals is coupled. Therefore, accurate estimation

of pressure profiles in build sections and main wellbore is important in order to predict the performance of a multilateral well accurately.

For a single-phase incompressible liquid flowing in a non-producing pipe, the pressure drop in the build section can be accounted for by calculating both the frictional pressure drop and the potential energy (hydrostatic) pressure drop, which can be represented by

$$\Delta p = p_1 - p_2 = \Delta p_f + \Delta p_{PE} \tag{2.19}$$

where Δp_f is the frictional pressure drop and Δp_{PE} is the potential energy pressure drop defined respectively as

$$\Delta p_f = \frac{2 f_f \rho u^2 L_m}{g_c d} \tag{2.20}$$

and

$$\Delta p_{PE} = \frac{g}{g_c} \rho L_v \tag{2.21}$$

L_m is the measured length of the build section and it is represented by the difference in the measured depths of the bottom and top points of the section, whereas L_v is the difference in elevation between the two points and it is represented by the vertical depth of the upstream point minus the vertical depth of the downstream point (Hill et al. 2008).

Two-phase flow may occur in the wellbore either because the reservoir is saturated, i.e., the reservoir pressure is below the bubble point, or gas may come out of solution after oil enters the wellbore due to the drop in flowing bottomhole pressure

below the bubble point. In either case, pressure drop for two-phase flow along the laterals and build sections must be considered for accurate wellbore modeling.

Many correlations have been published to account for two-phase flow in wellbores. However, they are only applicable for either vertical flow or horizontal flow. Very few correlations on the other hand such as the Beggs and Brill (1973) correlation, are capable of handling all flow directions, i.e., uphill, downhill, inclined and horizontal flow.

2.3 Coupling Reservoir and Wellbore Model

The pressure drop along horizontal laterals is calculated by coupling the reservoir inflow model with the wellbore pressure drop model. This is done by dividing the wellbore and reservoir into *n* number of segments from the toe to the heel of the wellbore as shown in **Figure 2.4**. Starting at the toe, the productivity of the segment is calculated using the reservoir inflow model and assuming a value for the flowing wellbore pressure, $p_{wf,1}$. Moving toward the heel, the wellbore pressure drop in the second segment is calculated by applying the wellbore pressure drop model. After that, the resulted pressure drop value is subtracted from the wellbore flowing pressure as shown from the following general equation

$$p_{wf,n} = p_{wf,n-1} - \Delta p_{n,n-1} \tag{2.22}$$

where $\Delta p_{n,n-1}$ is the wellbore pressure drop between segments *n* and *n*-1.

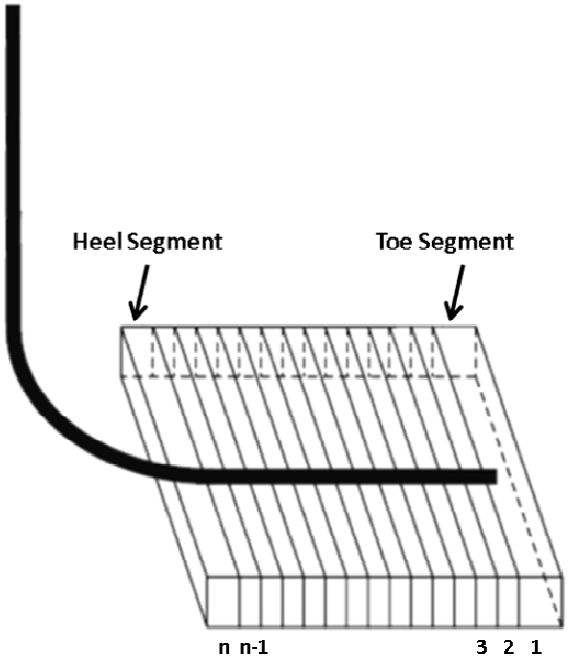

Figure 2.4: Geometry of reservoir and wellbore coupled model.

Using the new wellbore pressure value, $p_{wf,n}$, the flow rate of the next segment is calculated with the new drawdown pressure. Now, the pressure and flow rate for each segment are identified by repeating the same steps until reaching the heel of the wellbore. The total flow rate of the horizontal lateral is the sum of flow rates of all segments (Kamkom and Zhu 2005b).

3. INTELLIGENT WELLS

Intelligent well technology is one of the most significant breakthroughs in modern petroleum production technologies. It allows operators to remotely control production of multilateral wells without intervention, thereby, optimizing production, and maximizing recovery and capital-expenditure efficiency while minimizing operating costs (Robinson 2003). Some applications of this technology include managing production where there are significant variations among laterals in reservoir pressure, productivity, gas/water fractions, or permeability due to presence of fractures and faults (Mubarak et al. 2009).

Intelligent wells consist of downhole valves referred to as inflow control valves (ICV). A schematic of the intelligent completion is shown in **Figure 3.1**. The ICVs are classified according to the type of flow control they provide as binary, multi-position or infinitely variable. Binary valves provide the option of either allowing the flow or not, i.e., on or off. Multi-position valves provide several steps of choking. Infinitely variable valves are more advanced since they are equipped with sensors that provide the option of adjusting to the correct choking based on preset criteria (Silva 2007).

Another important component of the intelligent well system is the permanent downhole monitoring gauges which record and transmit real-time pressure and temperature data. In complex multilateral well configurations, such data can be utilized to obtain invaluable information about the well performance.

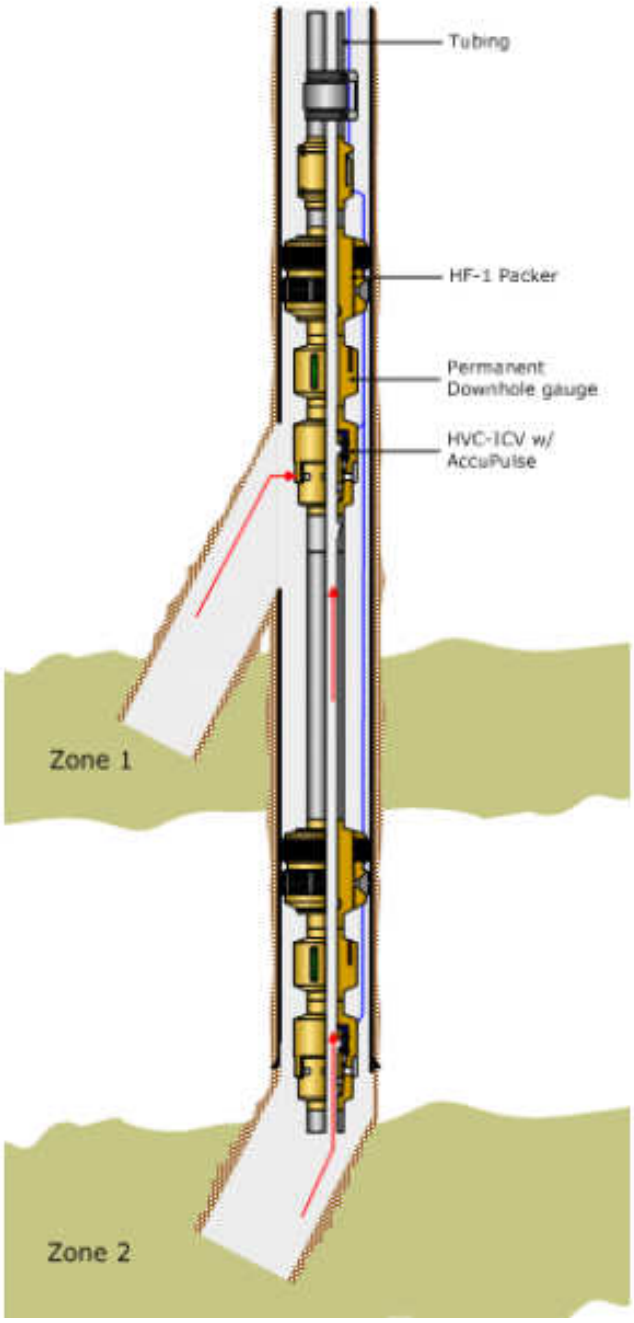

Figure 3.1: Downhole schematic of an intelligent completion (Ajayi et al. 2005).

3.1 Inflow Control Valve Design

The design of inflow control valves in intelligent wells is critical to achieve the desired objectives from the system. Several considerations come into account when deciding on the optimum design of ICV. In particular, the fully-open position of the valve must provide minimal pressure drop in order not to impose any restriction to the flow. In addition, other valve positions must be sensitive to controlling the flow when adjusted. This will provide a means to better optimize the production when water or gas begin to encroach on oil production, and to better deplete the reservoir by balancing the flow rates from individual laterals or zones according to the reservoir management plan. Therefore, there is no uniform design that can be generalized for all control valves.

The multi-position and infinite variable ICVs consist of a number of inflow ports positioned linearly as shown in **Figure 3.2**. The opening and closing of the ports is controlled by a sliding sleeve which can be actuated by either a hydraulic, electric or hybrid electro-hydraulic method. In the fully-open position (100% valve position), all ports are opened as shown in the middle diagram of **Figure 3.2**. The diagram to the left shows an ICV in the second position (20% valve position) where only two ports are opened. The flow area at each position is the cumulative area of all opened ports (Al-Mubarak et al. 2008).

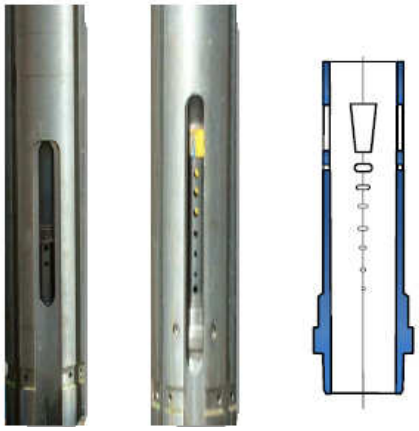

Figure 3.2: Inflow ports in the downhole control valve (Al-Mubarak et al. 2008).

When designing an ICV, the maximum anticipated flow rate from the lateral or zone must be considered. This is usually the flow rate corresponding to the lowest flowing bottomhole pressure taking into consideration the tubing performance. Combining the inflow performance relationship (IPR) curve with the tubing performance curve (TPC) will facilitate finding the operating equilibrium point which represents the maximum anticipated flow rate (**Figure 3.3**). The determined maximum rate is the flow rate of which 100% valve position should be capable of handling. The pressure drop across the ICV at this position should be almost negligible. At flow rates lower than the maximum, the pressure drop across the ICV should equal to the pressure difference between the IPR and TPC represented by Δp in **Figure 3.3** (Konopczynski and Ajayi 2004).

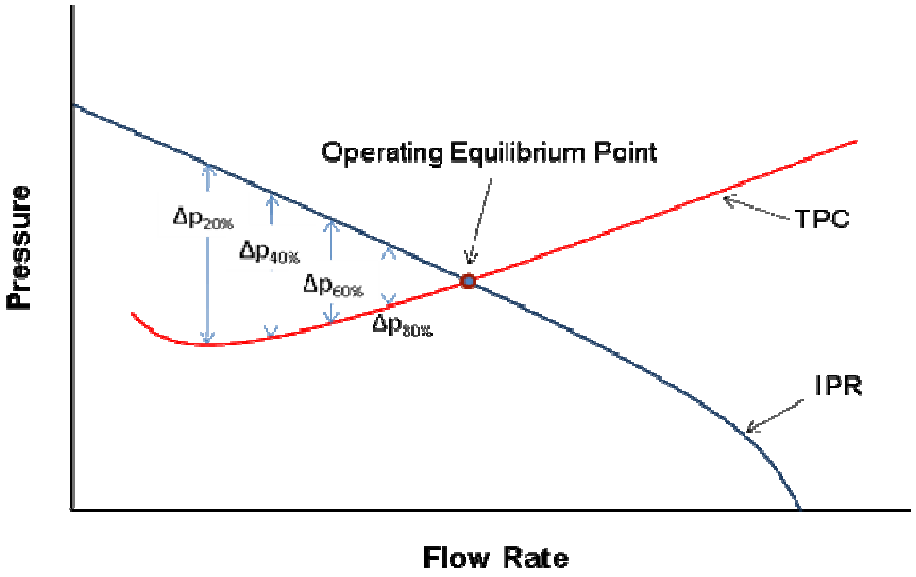

Figure 3.3: Combination of inflow performance relationship (IPR) and tubing performance curve (TPC).

The design of the flow control trim is a complex process that cannot be described with a single equation. Each valve position has a unique port size and geometry that can satisfy the required pressure drop. In addition, the design process may consider multi-phase flow. Therefore, the final ICV design is derived from a combination of analytical models, empirical correlations and flow loop testing (Konopczynski and Ajayi 2004).

The main parameter that distinguishes the flow performance of the ICV is the valve flow coefficient, C_v, which expresses the flow capacity in terms of water flow. The use of C_v is a convenient method to allow different control valves to be compared (Crane 1982).

It is desirable to achieve a linear flow control profile when designing an ICV, i.e., at a 40% valve position, the flow rate through the valve will be approximately 40%

of the design maximum rate, and at a 60% valve position, the flow rate will be approximately 60%, and so on. However, a linear flow control design is not always applicable. Due to economical and operational considerations, some operators tend to develop an optimized ICV design that can be applied not only for one well, but for the entire field.

3.2 Flow through Inflow Control Valves

Depending on the ICV's trim design and position setting, significant pressure loss may occur when the fluid passes through the restriction. Although they function differently, ICVs and surface choke valves are very similar in how they place restriction to the flow (**Figure 3.4**). Hence, the published equations that describe the flow through surface choke valves can be applied to ICVs with some modifications to account for the differences between surface and downhole conditions.

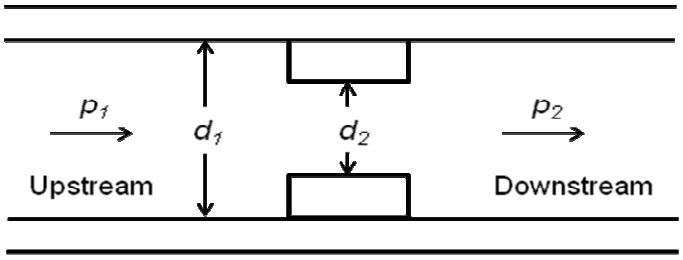

Figure 3.4: Choke schematic.

The flow through a restriction may be either critical or subcritical. At critical flow, the velocity of the fluid reaches a maximum value with respect to the upstream

conditions. This velocity reaches the sonic velocity, which is the reason critical flow is also called “sonic” flow. Under critical flow condition, pressure disturbance downstream of the restriction does not affect the pressure upstream, and thus, will not impact the flow rate (Beggs 2003). However, if the downstream pressure is increased to reach beyond the critical-subcritical flow boundary, both the upstream pressure and flow rate will be affected. The flow velocity through the restriction in this case falls below the sonic velocity which characterizes the subcritical flow behavior (Sachdeva et al. 1986).

3.2.1 Single-Phase Liquid Flow

The flow through restrictions for single-phase liquid will usually be subcritical. To relate the flow rate to the pressure drop across the restriction, the following relationship is used

$$q_L = C\, A_{choke} \sqrt{\frac{2 g_c\, \Delta p}{\rho}} \tag{3.1}$$

where C is the choke flow coefficient and A_{choke} is the cross-sectional area of the choke. **Eq. 3.2** can be written in field units as

$$q_L = 22{,}800 C (D_2)^2 \sqrt{\frac{\Delta p}{\rho}} \tag{3.2}$$

where D_2 is the restriction diameter (Economides et al. 1993). The term C is the choke flow coefficient which can be calculated by

$$C = \frac{C_d}{\sqrt{1-\beta^4}} \tag{3.3}$$

where C_d is the discharge coefficient, and β is the ratio of small to large diameters in a restriction ($\beta = D_2 / D_1$). The choke flow coefficient can be also obtained from **Figure 3.5**.

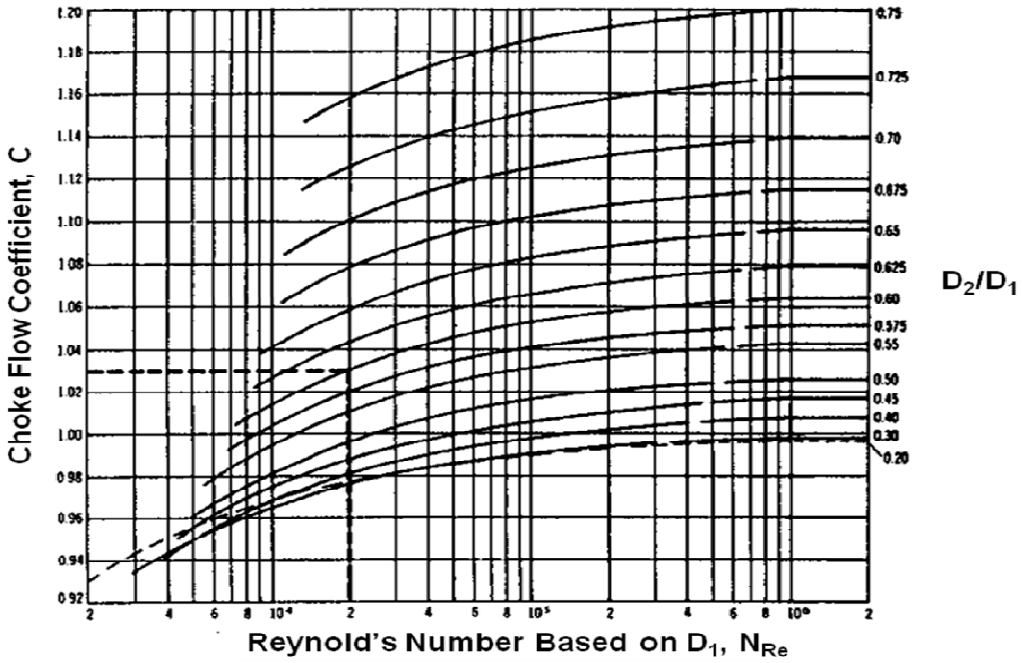

Figure 3.5: Choke flow coefficient for liquid flow through chokes (Crane 1982).

Single-phase liquid flow through restrictions can be also described in terms of the valve flow coefficient, C_v, which is determined in a test bench using water flow. C_v is described in units of US gallon/minute/psi$^{1/2}$ and is defined as

$$C_v = q_L \sqrt{\frac{\gamma_L}{\Delta p}} \tag{3.4}$$

where q_L is the liquid flow rate through the valve in US gallon per minute, and Δp represents the pressure drop across the choke valve in psi (Crane 1982).

3.2.2 Two-Phase Flow

Unlike single-phase liquid flow through restrictions, two-phase flow modeling is complex. It may occur as a critical or subcritical flow. The first step to model the flow rate-pressure drop relationship through restrictions such as ICVs is to define the boundary between critical and subcritical flow.

Sachdeva et al. (1986) developed an equation to calculate the critical-subcritical boundary for horizontal two-phase separated flow based on the equations describing the conservation of mass, momentum and energy. The model assumes the following:

- Flow is horizontal
- Phase velocities are equal at the throat, i.e., no slippage exists
- The liquid phase is incompressible
- The process is fast, therefore, there is no time for phase change
- Gas expansion is polytropic, i.e., $p_2 . V_{G2}^n = const.$

Sun, Konopczynski and Ajayi (2006) improved Sachdeva et al. model to account for the impact of different flow areas of the choke valve on the critical-subcritical boundary. They presented the following critical-subcritical boundary equation which can be solved for the critical pressure ratio, y_c

$$V_{G1}.y_c^{\frac{-1}{n}}.x_g\left(\frac{n}{n-1}\right)\left[1-\left(\frac{1}{y_c}\right)^{\frac{n-1}{n}}\right]+V_L\left(1-x_g\right)\left(1-\frac{1}{y_c}\right)$$
$$-\frac{n\left(\alpha^2-1\right)\left[x_g\left(V_{G1}\cdot y_c^{\frac{-1}{n}}-V_L\right)+V_L\right]^2}{2\cdot x_g\cdot V_{G1}\cdot y_c^{\frac{-1}{n}}}=0 \qquad (3.5)$$

where the gas polytropic exponent, n, is assumed to be identical to the gas specific heat ratio, k, ($k = C_p/C_v$). The gas specific volume at upstream, V_{G1} (ft^3/lb_m), can be determined using the gas low based on upstream pressure and temperature. The velocity ratio of upstream to downstream, α, is defined as

$$\alpha=\frac{A_{ICV}}{A_{annulus}}\left(\frac{V_{G1}\cdot x_g+V_L\cdot\left(1-x_g\right)}{V_{G1}\cdot y^{\frac{-1}{n}}\cdot x_g+V_L\left(1-x_g\right)}\right) \qquad (3.6)$$

After solving **Eq. 3.5** for the critical pressure ratio, y_c, the resulted value is compared to the actual downstream to upstream pressure ratio, y_a:

If $y_a \le y_c$, then the flow is critical and $y = y_c$, whereas if $y_a > y_c$, then the flow is subcritical and $y = y_a$.

Once the flow boundary is determined, the mass flow rate downstream of the ICV, M_2 (lbm/sec), can be determined by the following equation, which is applicable for both the critical and subcritical flow rates:

$$M_2 = A_{ICV} \cdot \left\{ \frac{288 g_c \cdot p_1}{\left(\alpha^2 - 1\right) \cdot \left[x_g \left(V_{G1} \cdot y^{\frac{-1}{n}} - V_L \right) + V_L \right]^2 \cdot \left[V_{G1} \cdot y^{\frac{-1}{n}} - x_g \cdot \frac{n}{n-1} \cdot \left(y - y^{\frac{-1}{n}} \right) + V_L \left(1 - x_g\right)\left(y - 1\right) \right]} \right\}^{\frac{1}{2}} \tag{3.7}$$

A step further in modeling two-phase flow through ICVs is to account for the change in phase behavior. This can be done by integrating fluid properties, real-time downhole data and surface production data. The upstream mass fractions of oil, free gas and water can be calculated using the following equations:

$$x_o = \frac{5.615 \rho_{o1} \cdot B_o}{\lambda + 5.615 \rho_{o1} \cdot B_o + 350.376 \gamma_w \cdot WOR \cdot B_w} \tag{3.8}$$

$$x_g = \frac{\lambda}{\lambda + 5.615 \rho_{o1} \cdot B_o + 350.376 \gamma_w \cdot WOR \cdot B_w} \tag{3.9}$$

$$x_w = 1 - x_o - x_g \tag{3.10}$$

where x_o, x_g and x_w represent the weight fractions of each phase upstream of the ICV. The term, λ, in **Eq. 3.8** and **3.9** is a gas parameter group in units of (lb_m/STB). λ is defined as

$$\lambda = 0.0765 \gamma_g \left(GOR - R_s - WOR \cdot R_{sw} \right) \tag{3.11}$$

Considering the principle of material balance, the production rate at the surface should equal to the mass flow rate through the ICV for steady-state flow. Therefore, the

calculated mass flow rate, M_2, can be converted to volumetric flow rate for each phase in field units as follows:

$$Q_w = 247\left(\frac{M_2 \cdot x_w}{\gamma_w}\right) \tag{3.12}$$

$$Q_o = 15387\left(\frac{M_2 \cdot x_o}{\rho_{o1} \cdot B_o}\right) \tag{3.13}$$

$$Q_g = 1.129\left(\frac{M_2 \cdot x_g}{\gamma_g}\right) + \frac{Q_o \cdot R_s}{10^6} + \frac{Q_w \cdot R_{sw}}{10^6} \tag{3.14}$$

(Sun et al. 2006).

4. CROSS-FLOW EVALUATION

Cross-flow is a common problem in multilateral well systems. When production is commingled, the produced fluid from one lateral will flow into other laterals due to large variances in layer productivities, pressures and drive mechanisms, which result in variation in bottomhole flowing pressures at the joints between laterals (Zhu and Furui 2006). Depending on the pressure variation, cross-flow may result in choking the production of other laterals, or entirely kill their production, processes that will negatively affect the overall well productivity.

Although proper well planning may prevent the cross-flow problem initially, changes encountered during the life of the multilateral well, such as reservoir pressure decline and water or gas encroachments in one of the laterals, may result in a cross-flow problem. Hence, the solution to this problem is to sequentially produce the zones, which requires physical intervention through shifting a sleeve via wire line or coiled tubing, or even considering a work-over to modify the well completion. Another option to resolve the cross-flow problem is to alter the bottomhole flowing pressures at the affected laterals. However, this option requires that the well is equipped with special equipment such as the intelligent completion, to control individual zones without physical intervention. ICVs can be operated to choke off the flow rate as desired to control the bottomhole flowing pressure at each lateral.

This study uses a typical example of a cross-flow problem to demonstrate the importance of intelligent completions in resolving this issue. The selected case is for a

heterogeneous tight reservoir where the performance of an MRC multilateral oil well is evaluated to investigate the cross-flow issue. After that, an intelligent well with the same properties of the first multilateral well is evaluated where ICVs are utilized to balance the pressures in order to resolve the cross-flow problem. The reservoir and wellbore flow performance are evaluated using the previously presented models.

In the presented example, the multilateral well consists of three horizontal laterals (tri-lateral) drilled in the same reservoir (**Figure 4.1**). All laterals have the same openhole length and wellbore diameter. The motherbore (Lateral-1) is drilled to the total required measured depth, and then it is cased and cemented. After that, a window is drilled and milled through the casing to drill the second lateral (Lateral-2). Similarly, a second window is drilled and milled to drill the third lateral (Lateral-3). Finally, the well is completed by running the production tubing and any other additional accessories. This configuration represents a TAML Level 2 multilateral junction completion (Hill et al. 2008).

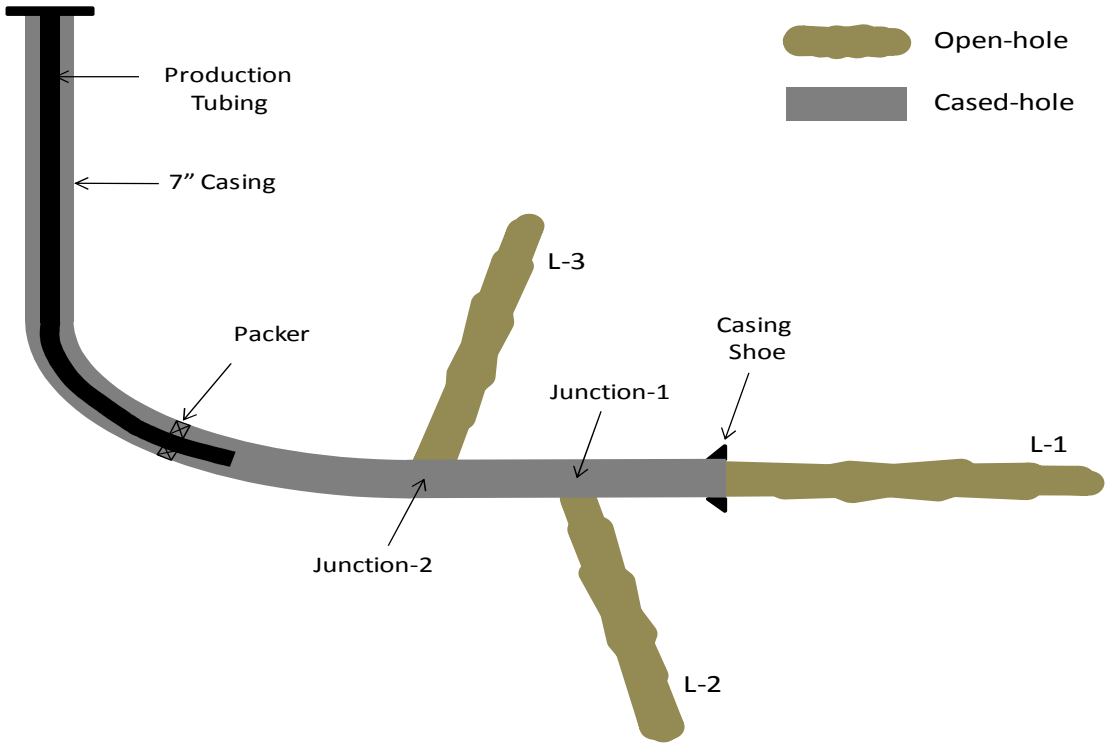

Figure 4.1: Multilateral well configuration.

The average reservoir pressure is 2500 psi with a permeability ranging between 10 and 60 md. Due to the reservoir heterogeneity, each lateral in this multilateral well has a different permeability. **Table 4.1** summarizes the reservoir and well properties for each lateral. To evaluate the well performance, the coupled reservoir and wellbore model is used for each lateral. This will account for the flow rate and pressure drop in the openhole section from the toe to the heel.

Table 4.1: Reservoir and wellbore properties for the multilateral well example

	Lateral-1	Lateral-2	Lateral-3	
Porosity, ϕ	0.24	0.24	0.24	frac.
Permeability, k_H	60	20	30	md
Permeability, k_V	6	2	3	md
Reservoir thickness, h	50	50	50	ft
Wellbore radius, r_w	0.255	0.255	0.255	ft
Avg. reservoir pressure, p_{avg}	2500	2500	2500	psi
Skin factor, s	0	0	0	-
Wellbore length, L	5500	5500	5500	ft
Viscosity, μ	1	1	1	cp
Volume factor, B	1.4	1.4	1.4	bbl/stb
Fluid density, ρ	55.0	55.0	55.0	lbm/ft^3
Drainage length	6100	6100	6100	ft
Drainage width	600	600	600	ft
Wellbore Relative Roughness, ε	0.0100	0.0100	0.0100	-
Openhole diameter, D	6.125	6.125	6.125	in
Flowing press at the toe, p_{wf}	2300	2300	2300	psi
Production angle, θ	0	0	0	^{o}
Total gas-oil ratio, GOR	0	0	0	scf/stb

For Lateral-1, the wellbore is divided into 15 segments. Starting at the toe segment, the productivity is calculated by Babu and Odeh reservoir inflow model (**Eq. 2.1**) using a flowing pressure, $p_{wf,1}$, value of 2300 psi. The calculated flow rate at the first segment, q_1, is 1014.6 bbl/d. Next, the wellbore pressure drop is calculated between the first and second segments accounting for the wall inflow effects by using Ouyang

wellbore pressure drop model (**Eq. 2.11**). The calculated pressure drop is 0.2 psi. After that, the wellbore pressure drop value at the second segment, $p_{wf,2}$, is calculated by **Eq. 2.22**, where it equals to 2299.8 psi. Then, the flow rate at the second segment, q_2, is calculated similar to the first segment, however, the total flow rate at the second segment will consist of the cumulative flow rates of q_1 and q_2. The steps are repeated until reaching the heel segment where the total flow rate is the sum of the flow rates of the 15 segments and the flowing pressure at the heel accounts for the cumulative pressure drop of all segments in the lateral. Similarly, the total flow rate and wellbore pressure drop are calculated for the other laterals in the well. The calculated results are summarized in **Table 4.2**.

Table 4.2: Summary of results for the coupled reservoir and wellbore model

	Lateral-1	Lateral-2	Lateral-3	
Wellbore press drop (openhole), Δp	63.8	5.8	12.9	psi
Total oil flow rate, q	18451.1	5268.1	7963.3	bbl/d
Flowing press at the heel, p_{wf}	2236.2	2294.2	2287.1	psi

The pressure drop inside the casing is calculated using the wellbore pressure drop model for a standard pipe (**Eq. 2.10**) with a pipe diameter of 7” and a relative roughness of 0.0006. Due to the relatively large pipe diameter, the pressure drop inside the casing is negligible and has no effect on the overall pressure between the laterals. **Figure 4.2** shows the IPR curve for each lateral treated individually without considering the effect of commingled production.

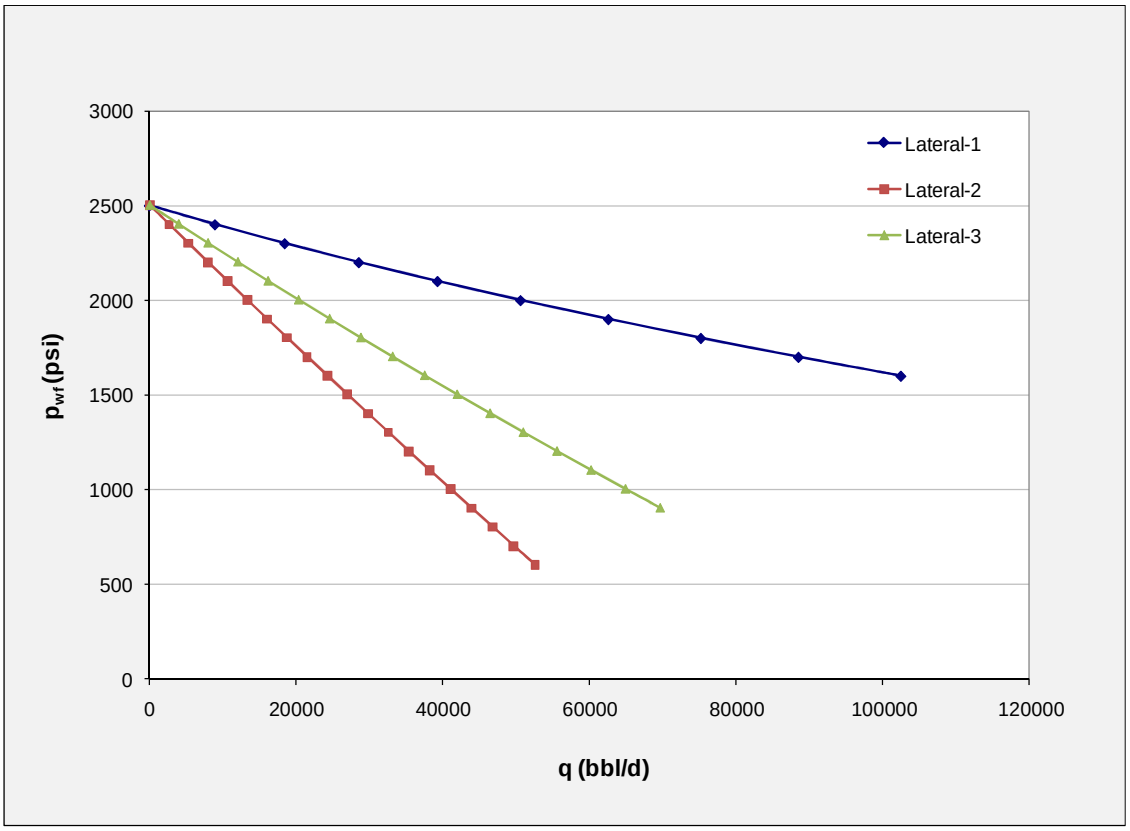

Figure 4.2: Individual lateral IPR curves (not commingled).

The flowing pressure at the heel of Lateral-2, represented by Junction-1 in **Figure 4.1**, is higher than the flowing pressure at the heel of Lateral-1. This will result in a restriction to the flow of Lateral-1. Depending on the surface wellhead operating pressure, which has not been considered in this example, the restriction to the flow of Lateral-1 can be either partial or complete. A significant production loss will be encountered in this case due to Lateral-1 being the most productive among the three laterals.

Considering the same multilateral well but with an installed 3-½" intelligent completion that has three multi-position ICVs of linear design performance. Each ICV controls the production from one lateral. The three zones are separated by packers **(Figure 4.3)**.

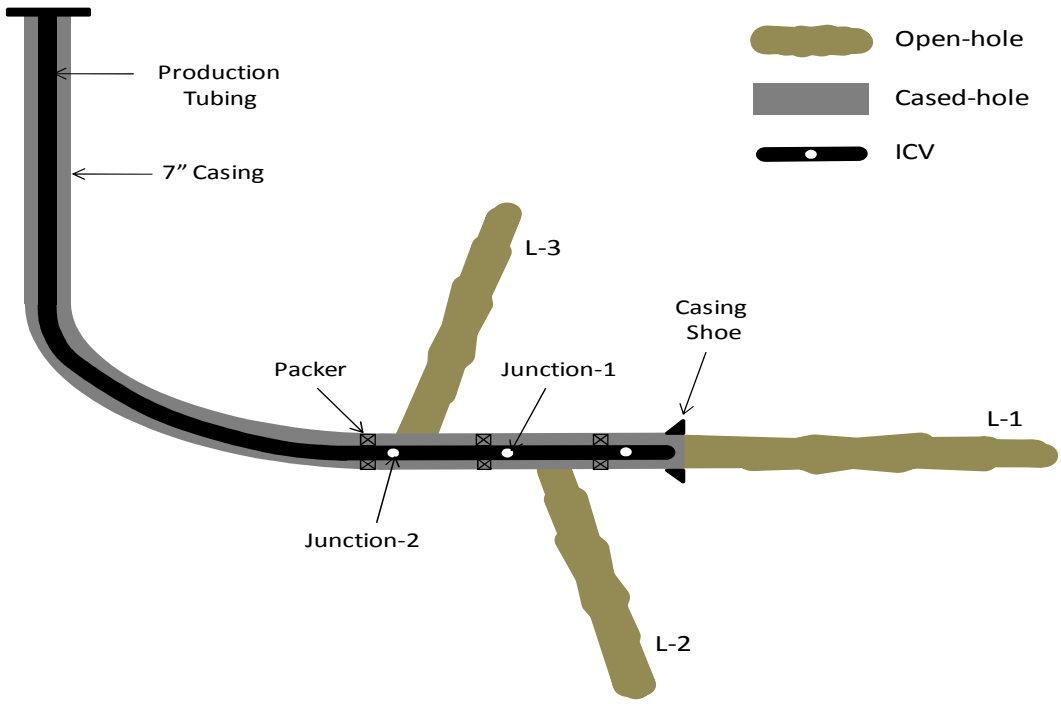

Figure 4.3: Intelligent well configuration.

Similar to the multilateral well, the well performance of each lateral is evaluated using the coupled reservoir and wellbore model. This yields the same results presented in **Table 4.2** since the reservoir and wellbore parameters are the same. However, in the intelligent well case, the pressure and flow rate values represent the conditions upstream of each corresponding ICV prior to commingling the production. Based on the flow

performance of each lateral, the pressure drop across each ICV can be calculated for each valve position using the single-phase liquid flow through ICV equation (**Eq. 3.4**). For example, the pressure drop across the ICV for Lateral-1 when the ICV is at position-9 is calculated as follows. Since the ICV has a linear flow performance, the ICV at position-9 will yield around 90% of the total flow rate upstream of the ICV (18,451 x 90% = 16,606 bbl/d). Arranging **Eq. 3.4**, the pressure drop across the ICV can be calculated in terms of the valve flow coefficient, C_v, which equals to 99.7 at this ICV position.

$$\Delta p = \gamma_L \left(\frac{q_L}{C_v} \right)^2 = \frac{55.0}{62.43} \left(\frac{16606 \times (42 \div (24 \times 60))}{99.7} \right)^2 = 20.8 \text{ psi}$$

Similarly, the pressure drop at each ICV position can be calculated. The results for Lateral-1,2 and 3 ICV performance are shown in **Tables 4.3**, **4.4** and **4.5**, respectively.

Table 4.3: ICV performance for Lateral-1

ICV Position	Pressure Drop Across ICV (psi)	ICV Open Area (in^2)	%of Open Area	Flow Rate (bbl/d)
1	21086.5	0.04	0.9%	1845
2	8859.2	0.08	2.0%	3690
3	3953.7	0.15	3.6%	5535
4	2207.1	0.23	5.6%	7380
5	1443.8	0.31	7.6%	9226
6	748.6	0.47	11.5%	11071
7	276.8	0.83	20.4%	12916
8	113.5	1.22	30.1%	14761
9	20.8	2.52	62.1%	16606
10	8.3	4.06	100.0%	18451

Table 4.4: ICV performance for Lateral-2

ICV Position	Pressure Drop Across ICV (psi)	ICV Open Area (in^2)	%of Open Area	Flow Rate (bbl/d)
1	2085.2	0.04	0.9%	580
2	876.1	0.08	2.0%	1160
3	391.0	0.15	3.6%	1741
4	218.3	0.23	5.6%	2321
5	142.8	0.31	7.6%	2901
6	74.0	0.47	11.5%	3481
7	27.4	0.83	20.4%	4062
8	11.2	1.22	30.1%	4642
9	2.1	2.52	62.1%	5222
10	0.8	4.06	100.0%	5802

Table 4.5: ICV performance for Lateral-3

ICV Position	Pressure Drop Across ICV (psi)	ICV Open Area (in^2)	%of Open Area	Flow Rate (bbl/d)
1	4779.5	0.04	0.9%	878
2	2008.0	0.08	2.0%	1757
3	896.2	0.15	3.6%	2635
4	500.3	0.23	5.6%	3514
5	327.3	0.31	7.6%	4392
6	169.7	0.47	11.5%	5271
7	62.7	0.83	20.4%	6149
8	25.7	1.22	30.1%	7028
9	4.7	2.52	62.1%	7906
10	1.9	4.06	100.0%	8784

Using the ICV performance results and accounting for the frictional pressure losses inside the 3-1/2" horizontal tubing, ICVs are adjusted to equalize the pressure at Junction-1 and 2 and prevent any cross-flow. If Lateral-1 is being produced at ICV position-8, the expected flow rate downstream of Lateral-1 ICV is 14761 bbl/d as calculated in the ICV performance table. With this flow rate, the wellbore pressure drop

of the 610 ft section inside the tubing between Lateral-1 and 2 can be calculated using the wellbore pressure drop model for a standard pipe (**Eq. 2.10**) with a pipe diameter of 3-1/2" and a relative roughness of 0.0006.

$$\Delta p = p_1 - p_2 = \frac{g}{g_c}\rho L_s \sin\theta + \frac{2 f_f \rho u^2 L_s}{g_c d}$$

Since the wellbore is horizontal (θ = 0), there will be no gravitational effects. Hence, the pressure drop will consist of only a frictional pressure drop term.

Reynolds number is calculated in oilfield units:

$$N_{\mathrm{Re}} = \frac{1.48 q\rho}{d\mu} = \frac{1.48(14761\,\mathrm{bbl/d})(55.0\,\mathrm{lb_m/ft^3})}{(3.5\,\mathrm{in})(1.0\,\mathrm{cp})} = 343{,}298$$

The friction factor is determined using Chen equation:

$$\frac{1}{\sqrt{f_f}} = -4\log\left\{\frac{\varepsilon}{3.7065} - \frac{5.0452}{N_{\mathrm{Re}}}\log\left[\frac{\varepsilon^{1.1098}}{2.8257} + \left(\frac{7.149}{N_{\mathrm{Re}}}\right)^{0.8981}\right]\right\}$$

$$\frac{1}{\sqrt{f_f}} = -4\log\left\{\frac{0.0006}{3.7065} - \frac{5.0452}{343298}\log\left[\frac{0.0006^{1.1098}}{2.8257} + \left(\frac{7.149}{343298}\right)^{0.8981}\right]\right\}$$

$$f_f = 0.0047$$

$$u = \frac{4q}{\pi d^2} = \frac{4(14761\,\mathrm{bbl/d})(5.615\,\mathrm{ft^3/bbl})(1\mathrm{d}/86400\,\mathrm{s})}{\pi[(3.5/12)\mathrm{ft}]^2} = 14.36\,\mathrm{ft/s}$$

$$\Delta p = \frac{2 f_f \rho u^2 L_s}{g_c d} = \frac{2(0.0047)(55.0\,\mathrm{lb_m/ft^3})(14.36\,\mathrm{ft/s})^2(610\,\mathrm{ft})}{(32.17\,\mathrm{ft\text{-}lb_m/lb_f\text{-}s^2})[(3.5/12)\mathrm{ft}]}\frac{1\,\mathrm{ft}^2}{144\,\mathrm{in}^2} = 48\,\mathrm{psi}$$

Knowing the flowing pressure downstream of the ICV of Lateral-1 and accounting for the wellbore frictional pressure drop inside the tubing, the pressure at Junction-1 can be determined as follows:

p_{wf} downstream of ICV = 2123 psi, and

Δp inside the tubing = 48 psi

Thus, the pressure at Junction-1 = 2123 psi – 48 psi = 2075 psi

Next, the flow rate of Lateral-2 is adjusted by modifying the ICV position to reach a flowing pressure downstream if the ICV equals to the pressure at Junction-1. Using the ICV performance table for Lateral-2, the ideal ICV position to meet the required pressure drop is position-4, which yields a pressure value of 2076 psi (p_{wf} upstream of ICV - Δp across ICV). Similarly, the same steps are repeated to determine the flowing pressure at Junction-2 and the required ICV adjustment for Lateral-3 that equalizes the pressure with Junction-2. However, to calculate the wellbore pressure drop between Junction-1 and 2, the cumulative flow rate of Lateral-1 and 2 has to be considered.

The optimized ICV positions for commingled production are listed in **Table 4.6**. In addition, the IPR curves for the commingled production at the current ICV settings are shown in **Figure 4.4**. The overall selection of ICV positions should match the reservoir management strategy of producing the reservoir.

Table 4.6: Summary of results for the intelligent well commingled production

	Lateral-1	Lateral-2	Lateral-3	
Flowing press upstream of ICV, p_1	2236	2294	2287	psi
Oil flow rate upstream of ICV, q_{l1}	18451	5268	7963	bbl/d
ICV position	8	4	5	
Flowing press downstream of ICV, p_2	2123	2076	2019	psi
Oil flow rate downstream of ICV, q_{l2}	14761	2107	3982	bbl/d
Pressure drop inside tubing L1-L2, Δp	48.0			psi
Pressure drop inside tubing L2-L3, Δp	58.1			psi
Flowing pressure at Junction-1	2075			psi
Flowing pressure at Junction-2	2019			psi
Total commingled oil rate, q_T	20850			bbl/d

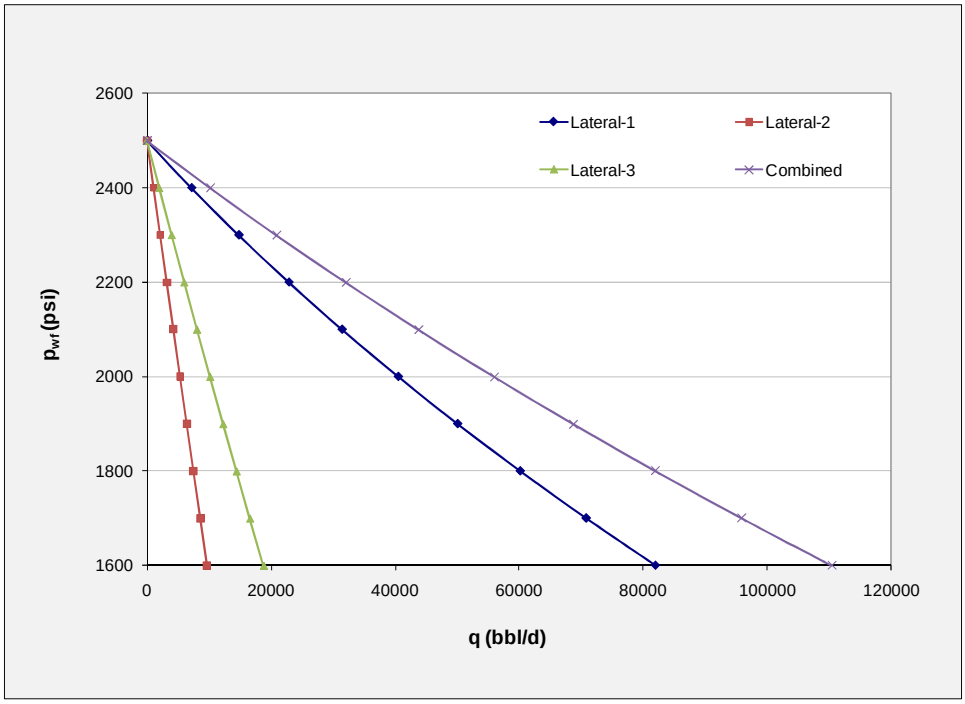

Figure 4.4: Intelligent well IPR curves for commingled production at selected ICV settings.

Cross-flow is a critical problem in intelligent wells when the production is commingled from multiple reservoirs or zones. Not only it will cause a restriction to the flow, but it might also cause the flow of unwanted fluids from one reservoir into another.

Surface choke valves can be utilized in conjunction with the ICVs to slightly adjust the rate if needed. Following this strategy will avoid the need to finding a new operating equilibrium point whenever one of the ICVs is adjusted (Konopczynski and Ajayi 2004).

5. CONCLUSIONS

Intelligent well applications have rapidly increased in the last decade. They have been proven to improve hydrocarbon recovery. Wells equipped with intelligent completions are unconventional, complex, multilateral wells that require accurate performance evaluation. This thesis presents well performance models of horizontal and multilateral wells. In addition, it combines the performance models with flow through inflow control valve models to optimize the multilateral well performance. The common cross-flow problem in multilateral wells can be easily prevented by accurately evaluating the flowing pressure at the junctions between the laterals and then adjusting the ICVs to reach an optimum operating pressure. The use of permanent downhole pressure and temperature gauges, part of the intelligent completion system, is essential when modeling two-phase flow. However, accurate placement of these gauges based on the intelligent well application is crucial to get the most out of them.

NOMENCLATURE

A	flow or drainage area, ft^2
a	reservoir length in the direction perpendicular to a horizontal lateral, ft
$A_{Annulus}$	flow area at upstream of ICV, ft^2
A_{choke}	cross-sectional area of the choke, ft^2
A_{ICV}	cumulative flow area of ICV at a specific valve position, ft^2
b	reservoir length in the direction of a horizontal lateral, ft
B_o	oil formation volume factor, res bbl/stb
B_w	water formation volume factor, res bbl/stb
C	choke flow coefficient
C_d	discharge coefficient
C_H	shape factor
C_p	specific heat of gas at constant pressure
C_v	specific heat of gas at constant volume
C_v	valve flow coefficient, $USgpm/psi^{1/2}$
d	pipe diameter, ft
D_2	restriction (choke) diameter, ft
f_f	fanning friction factor
f_f^*	friction factor for pipes with inflow
g	acceleration of gravity, ft/sec^2

g_c	gravitational constant, ft-lbf/lbm-sec^2
GOR	gas-oil ratio, scf/stb
h	reservoir thickness, ft
$Iani$	anisotropy index
J	productivity index, bbl/d/psi
kH	horizontal permeability, md
k_H	vertical permeability, md
k_x	permeability in the x-direction, md
k_y	permeability in the y-direction, md
k_z	permeability in the z-direction, md
L	horizontal well length, ft
L_m	measured length, ft
L_s	segment length of pipe, ft
L_v	vertical length, ft
M	mass flow rate, lb_m/sec
n	polytropic exponent for gas
N_{Re}	Reynolds number
$N_{Re,w}$	inflow Reynolds number
$\bar{p}$	average reservoir pressure, psi
p_1	pressure at upstream, psi
p_2	pressure at downstream, psi
p_{wf}	wellbore flowing pressure, psi

q	flow rate, bbl/d
$\bar{q}$	average flow rate in a lateral segment, bbl/d
q_g	gas flow rate, Mscf/d
Q_g	gas production rate in field units, stb/d
q_I	inflow rate into a lateral segment, bbl/d-ft
q_L	liquid flow rate, USgpm
q_o	oil flow rate, bbl/d
Q_o	oil production rate in field units, stb/d
$q_{o,max}$	maximum open flow potential, bbl/d
Q_w	water production rate in field units, stb/d
R_s	solution gas-oil ratio, scf/stb
R_{sw}	solution gas-water ratio, scf/stb
r_w	wellbore radius, ft
s	skin factor
s_R	partial penetration skin factor
u	flux or velocity, ft/min
V_{G1}	gas specific volume at upstream, ft^3/lbm
V_{G2}	gas specific volume at downstream, ft^3/lbm
V_L	liquid specific volume, ft^3/lb_m
WOR	water-oil-ratio
x_1	x-coordinate of one end of horizontal well location, ft
x_2	x-coordinate of other end of horizontal well location, ft

x_g	free gas quality at upstream (weight fraction of free gas)
x_{mid}	x-coordinate of midpoint of horizontal well location, ft
x_o	oil quality at upstream (weight fraction of oil)
x_w	water quality at upstream (weight fraction of water)
y	pressure ratio between downstream and upstream
y_0	y-coordinate of horizontal well location, ft
y_c	critical-subcritical pressure ratio
z_0	z-coordinate of horizontal well location, ft
α	velocity ratio of upstream to downstream
β	ratio of small to large diameters in a restriction
Δp	pressure drop, psi
Δp_f	frictional pressure drop, psi
Δp_{PE}	potential energy (hydrostatic) pressure drop, psi
ε	pipe roughness
ϕ	porosity, fraction
γ_w	relative density of formation water (water = 1)
γ_g	relative density of gas (air = 1)
γ_L	relative density of liquid (water = 1)
μ	viscosity, cp
ρ	density, lbm/ft^3
ρ_o	oil density, lb$_m$/ft^3

REFERENCES

Ajayi, A. A., Mathieson, D. and Konopczynski, M. R. 2005. An Innovative Way of Integrating Reliability of Intelligent Well Completion System with Reservoir Modelling. Paper SPE 94400-MS presented at the Offshore Europe, Aberdeen, United Kingdom, 6-9 September.

Al-Mubarak, S. M., Sunbul, A. H., Hembling, D. E., Sukkestad, T. and Jacob, S. 2008. Improved Performance of Downhole Active Inflow Control Valves through Enhanced Design: Case Study. Paper SPE 117634-MS presented at the Abu Dhabi International Petroleum Exhibition and Conference, Abu Dhabi, UAE, 3-6 November.

Babu, D. K. and Odeh, A. S. 1989. Productivity of a Horizontal Well (includes associated papers 20306, 20307, 20394, 20403, 20799, 21307, 21610, 21611, 21623, 21624, 25295, 25408, 26262, 26281, 31025, and 31035). *SPE Reservoir Engineering* **4** (4): 417-421.

Beggs, D. H. and Brill, J. P. 1973. A Study of Two-Phase Flow in Inclined Pipes. *SPE Journal of Petroleum Technology* **25** (5): 607-617.

Beggs, H. D. 2003. *Production Optimization Using Nodal Analysis*, Second Edition. Tulsa, Oklahoma: OGCI and Petroskills Publications.

Butler, R. M. 1994. *Horizontal Wells for the Recovery of Oil, Gas, and Bitumen*, Monograph No. 2, Petroleum Sos. of Canadian Institute of Mining, Metallurgy, and Petroleum.

Crane. 1982. *Flow of Fluids through Valves, Fittings, and Pipe - Metric Edition*. New York, NY: Crane Co.

Dossary, A. S. and Mahgoub, A. A. 2003. Challenges and Achievements of Drilling Maximum Reservoir Contact (MRC) Wells in Shaybah Field. Paper SPE 85307-MS presented at the SPE/IADC Middle East Drilling Technology Conference and Exhibition, Abu Dhabi, UAE, 20-22 October.

Economides, M. J., Hill, A. D. and Economides, C. E. 1993. *Petroleum Production Systems*. Upper Saddle River, NJ: Prentice Hall.

Furui, K., Zhu, D. and Hill, A. D. 2003. A Rigorous Formation Damage Skin Factor and Reservoir Inflow Model for a Horizontal Well (includes associated papers 88817 and 88818). *SPE Production & Operations* **18** (3): 151-157.

Guo, B., Lyons, W. C. and Ghalambor, A. 2007. *Petroleum Production Engineering, A Computer-Assisted Approach*. Burlington, MA: Gulf Professional Publishing.

Hill, A. D., Zhu, D. and Economides, M. J. 2008. *Multilateral Wells*. Richardson, TX: Society of Petroleum Engineers.

Joshi, S. D. 1988. Augmentation of Well Productivity With Slant and Horizontal Wells (includes associated papers 24547 and 25308). *SPE Journal of Petroleum Technology* **40** (6): 729-739.

Kamkom, R. and Zhu, D. 2005a. Evaluation of Two-Phase IPR Correlations for Horizontal Wells. Paper SPE 93986-MS presented at the SPE Production Operations Symposium, Oklahoma City, Oklahoma, USA, 16-19 April.

Kamkom, R. and Zhu, D. 2005b. Two-Phase Correlation Model for Multilateral Well Deliverability. Paper SPE 95652-MS presented at the SPE Annual Technical Conference and Exhibition, Dallas, Texas, USA, 9-12 October.

Kamkom, R. and Zhu, D. 2006. Generalized Horizontal Well Inflow Relationships for Liquid, Gas, or Two-Phase Flow. Paper SPE 99712-MS presented at the SPE/DOE Symposium on Improved Oil Recovery, Tulsa, Oklahoma, USA, 22-26 April.

Konopczynski, M. and Ajayi, A. 2004. Design of Intelligent Well Downhole Valves for Adjustable Flow Control. Paper SPE 90664-MS presented at the SPE Annual Technical Conference and Exhibition, Houston, Texas, USA, 26-29 September.

Konopczynski, M. R. and Ajayi, A. A. 2008. Reservoir Surveillance, Production Optimisation and Smart Workflows for Smart Fields - a Guide for Developing and Implementing Reservoir Management Philosophies and Operating Guidelines in Next Generation Fields. Paper SPE 112244-MS presented at the Intelligent Energy Conference and Exhibition, Amsterdam, The Netherlands, 25-27 February.

Mubarak, S., Dawood, N. and Salamy, S. 2009. Lessons Learned from 100 Intelligent Wells Equipped with Multiple Downhole Valves. Paper SPE 126089-MS presented at the SPE Saudi Arabia Section Technical Symposium, AlKhobar, Saudi Arabia, 9-11 May.

Ouyang, L.-B., Petalas, N., Arbabi, S., Schroeder, D. E. and Aziz, K. 1998. An Experimental Study of Single-Phase and Two-Phase Fluid Flow in Horizontal Wells. Paper SPE 46221-MS presented at the SPE Western Regional Meeting, Bakersfield, California, USA, 10-13 May.

Perkins, T. K. 1993. Critical and Subcritical Flow of Multiphase Mixtures Through Chokes. *SPE Drilling & Completion* **8** (4): 271-276.

Robinson, M. 2003. Intelligent Well Completions. *SPE Journal of Petroleum Technology* **55** (8): 57-59.

Sachdeva, R., Schmidt, Z., Brill, J. P. and Blais, R. M. 1986. Two-Phase Flow Through Chokes. Paper SPE 15657-MS presented at the SPE Annual Technical Conference and Exhibition, New Orleans, Louisiana, USA, 5-8 October.

Salamy, S. P., Mubarak, S., Mubarak, H., Dawood, N. J. and Al-Alawi, A. A. 2008. Maximum Reservoir Contact Wells: Six Years of Performance-Lessons Learned and Best Practices. Paper SPE 118030-MS presented at the Abu Dhabi International Petroleum Exhibition and Conference, Abu Dhabi, UAE, 3-6 November.

Silva, M. F., Pinto, H. L., Izetti, R. G. 2007. Intelligent Wells in Petrobras. *Brazil Oil & Gas* (7): 6-13.

Sun, K., Konopczynski, M. R. and Ajayi, A. A. 2006. Using Downhole Real-Time Data to Estimate Zonal Production in a Commingled-Multiple-Zones Intelligent System. Paper SPE 102743 presented at the SPE Annual Technical Conference and Exhibition, San Antonio, Texas, USA, 24-27 September.

Vogel, J. V. 1968. Inflow Performance Relationships for Solution-Gas Drive Wells. *SPE Journal of Petroleum Technology* **20** (1): 83-92.

Zhu, D. and Furui, K. 2006. Optimizing Oil and Gas Production by Intelligent Technology. Paper SPE 102104-MS presented at the SPE Annual Technical Conference and Exhibition, San Antonio, Texas, USA, 24-27 September.

VITA

Marwan Annas H Zarea received his Bachelor of Science degree in petroleum engineering from Montana Tech of the University of Montana in 2004. He entered the Harold Vance Department of Petroleum Engineering at Texas A&M University in August 2008 and received his Master of Science degree in August 2010.

Mr. Zarea can be reached at Saudi Aramco, P.O. Box: 11331, Dhahran 31311, Saudi Arabia.